Journal of Nuclear Medicine, published on April 16, 2015 as doi:10.2967/jnumed.114.152496

Claudin-4 SPECT imaging allows detection of aplastic lesions in a mouse model of breast cancer

Michael Mosley[1], James Knight[1], Albrecht Neesse[2], Patrick Michl[3], Manuela Iezzi[4], Veerle Kersemans[1], Bart Cornelissen[1,*]

[1] CR-UK/MRC Gray Institute for Radiation Oncology and Biology, University of Oxford, Oxford, United Kingdom

[2] Department of Gastroenterology II, University Medical Center, Georg-August University, Göttingen, Germany

[3] Department of Gastroenterology, Endocrinology, Infectiology and Metabolism, Philipps University Marburg, Marburg, Germany

[4] Department of Medicine and Aging Sciences, G. d'Annunzio University of Chieti-Pescara, Chieti, Italy

***To whom correspondence should be addressed:**
Dr. Bart Cornelissen
CRUK/MRC Oxford Institute for Radiation Oncology
Department of Oncology
University of Oxford
Old Road Campus Research Building
Off Roosevelt Drive
Oxford OX3 7LJ
Tel: +44 (0)1865 857126
Fax: +44 (0)1865 857127
Email: bart.cornelissen@oncology.ox.ac.uk

1st author: Michael Mosley, not currently in training
CRUK/MRC Oxford Institute for Radiation Oncology
Department of Oncology
University of Oxford
Old Road Campus Research Building
Off Roosevelt Drive
Oxford OX3 7LJ
Tel: +44 (0)1865 225840
Fax: +44 (0)1865 857127
Email: micheal.mosley@oncology.ox.ac.uk

Running Title: Claudin-4 SPECT imaging in breast cancer

Word count: 4994

Financial Support: This research was supported by a Cancer Research UK grant to G McKenna, the CRUK/EPSRC Cancer Imaging Centre in Oxford, and Deutsche Krebshilfe

ABSTRACT

Expression of claudin-4, a protein involved in tight junction complexes, is widely dysregulated in epithelial malignancies. Claudin-4 is overexpressed in a number of premalignant precursor lesions, including those of cancers of the breast, pancreas and prostate, and is associated with poor survival. A non-cytotoxic c-terminal fragment of *Clostridium perfringens* enterotoxin (cCPE) is a natural ligand for claudin-4. Here, we demonstrate whole-body quantitative SPECT imaging of preneoplastic breast cancer tissue using ^{111}In-labelled cCPE.

Methods cCPE.GST or GST was conjugated to the metal ion chelator, benzylDTPA, to allow ^{111}In radiolabelling. Affinity of radiolabelled cCPE.GST for claudin-4 was confirmed using claudin-4 expressing MDA-MB-468 and SQ20b cells, compared to claudin-4 negative HT1080 cells. In vivo SPECT imaging was performed using athymic mice bearing MDA-MB-468 or HT1080 xenografts, and using genetically modified *balb/neuT* mice, which spontaneously develop claudin-4-expressing breast cancer lesions.

Results Uptake of ^{111}In-cCPE.GST in claudin-4 positive MDA-MB-468 xenograft tumors in athymic mice was significantly higher compared to ^{111}In-GST or claudin-4 negative HT1080 tumors (6.72±0.18 vs. 3.88±1.00 vs. 2.36±1.25 %ID/g; P<0.0001). No other significant differences were observed in any of the examined organs. *Balb/neuT* mice, expressing rat *neuT* under *mmtv* promotor control, spontaneously develop tumorous lesions within their mammary fat pads over the course of 130 days. Overt mammary tumors were claudin-4 positive, and ^{111}In-cCPE.GST uptake was 3.2±0.70 %ID/g, significantly higher than ^{111}In-GST (1.00±0.60 %ID/g; P<0.05). Mammary fat pads in mice aged 80 days, bore claudin-4 positive aplastic lesions and accumulated ^{111}In-cCPE.GST (3.17±0.51 %ID/g), but not ^{111}In-GST (0.99±0.39 %ID/g; P <0.001).

Conclusion Taken together, ^{111}In-cCPE.GST targets claudin-4 expression in frank tumors and preneoplastic tissue, and cCPE imaging may be used as an early detection tool for breast, prostate, and pancreatic cancer.

Key words: claudin-4, cCPE, SPECT, tumorigenesis, breast cancer

INTRODUCTION

Early detection of cancer greatly increases the chances for successful treatment and long-term survival, and early diagnosis of cancer by medical imaging is certainly the major contributor to a reduction in mortality for breast cancer over the last decade (http://www.who.int), (*1*). Even though the ability to detect precancerous lesions would even further improve the facility for early intervention and improved patient outcome, to date, few effective imaging methods exist to detect precancerous lesions. Here, we propose that molecular imaging using SPECT of the increased expression of claudin-4 in pre-cancerous lesions of the breast has potential to improve early detection.

Claudin-4 is a 22 kDa member of the 27-member claudin protein family, and is a vital component in adherens and tight junction complexes (*2*). They are widely dysregulated in epithelial malignancies (*3*). Claudin-4 expression can be used to distinguish certain types of cancers (*4*), since it is overexpressed in a number of premalignant precursor lesions compared to normal tissue, including lesions in the pancreas (*5*), prostate (*6*), lung (*7*), colon (*8*), and breast (*3, 9, 10*), where claudin-4 overexpression is associated with poor prognosis. The exact mechanistic role of claudin-4 during tumorigenesis, and its role in solid tumours remains to be elucidated (*3*). Nevertheless, it can act as a valid clinical biomarker for early diagnosis, as laid out in a recent review by Kwon et al. on ovarian cancers (*3*). Also, Neesse et al. explored the possibility of claudin-4 targeting using fluorescently labelled proteins as imaging biomarkers in pancreatic cancer (*5*).

Imaging of claudin-4 has been shown by Neesse et al. to be an effective way to detect (pre-) cancerous lesions of the pancreas (*5*). *Clostridium perfringens* enterotoxin (CPE), which causes the symptoms of a very common food poisoning, is a natural ligand for claudin-4 (*11*). It is a single polypeptide of approximately 35 kDa in size, and is associated with type A food poisoning and such non-foodborne gastrointestinal diseases as antibiotic-associated diarrhoea and sporadic diarrhoea (*12*). The CPE receptor-binding activity of full-length CPE (319aa) is restricted to the 30 C-terminal amino acids (*13*). Recently,

site-directed mutagenesis revealed three Tyr residues, located at positions 306, 310 and 312 to be critical for receptor binding to claudin-4. Furthermore, competitive binding experiments showed that C-terminal CPE (cCPE, residues 184-319, 15 kDa) binds with 1:1 stoichiometry and submicromolar affinity to pure claudin-4. It's been shown that cCPE, is sufficient to bind claudin-4, but does not exert cytotoxicity since it lacks residues 80-106 necessary for membrane insertion and pore formation (*14*).

Neesse et al. used a Cy5.5-labelled glutathione S-transferase (GST)-tagged version of cCPE (cCPE.GST, 41 kDa), and showed excellent uptake in claudin-4 expressing xenografts, as well as claudin-4 expressing pancreatic tumors in an engineered mouse model of KRAS-mutation induced pancreatic ductal adenocarcinoma (PDAC). Earlier, Cocco et al. showed similar results using a FITC-conjugated cCPE in models of ovarian cancer (*15*). However, the direct clinical translation of optical imaging approaches is limited by penetration depth of light, which is less than a couple of millimetres. To overcome this obstacle, we have now labelled cCPE with the radionuclide ^{111}In which emits tissue-penetrating gamma rays that can be detected by non-invasive SPECT imaging.

Here, we present our results on ^{111}In-labelled cCPE.GST. We demonstrate the possibility of whole body, non-invasive imaging of claudin-4 expression in two models of breast cancer in mice. We further establish the possibility of early detection of pre-cancerous aplastic lesions in a mouse model of HER2-overexpressing breast adenocarcinoma.

MATERIALS AND METHODS

A COOH-terminal fragment of CPE (aa184-319) linked to a GST fusion protein has previously been produced by P. Michl (*5*). Purity was confirmed by SDS-PAGE gel (Supplementary Figure S1). A detailed procedure is laid out in the supplementary data. Purified cCPE.GST or GST was conjugated to benzyl-DTPA to allow radiolabelling with ^{111}In, as previously described (*16*). A detailed procedure is laid out in the supplementary data.

MDA-MB-468, SQ20b, and HT1080 human cancer cells were obtained from ATCC. Cells were tested and authenticated by the provider, using short tandem repeat profiling. The length of time in culture of these cells was less than 6 months after retrieval from liquid nitrogen storage. Cells were cultured in 5% CO_2 in DMEM cell culture medium (Sigma-Aldrich) supplemented with 10% fetal calf serum (Invitrogen), and penicillin/streptomycin, 100 units/mL (Invitrogen).

Aliquots of 2×10^5 MDA-MB-468, SQ20b, or HT1080 cells were seeded on coverslips and allowed to adhere overnight. To determine claudin-4 expression, and the ability of cCPE to bind, cells were washed twice with PBS, fixed for 10 min at room temperature with 4% paraformaldehyde (Sigma), blocked with 2% bovine serum albumin in phosphate buffered saline (PBS, pH 7.4) for 1 h, and incubated with mouse anti-claudin-4 antibodies (R&D systems, clone 382321, 1:400 dilution in blocking buffer) for 1 h at 37°C, and, following 3 washes, goat anti-mouse antibody (Invitrogen; 1:250 dilution) labeled with AlexaFluor594 for 1 h at 37°C, and mounted using Vectashield containing DAPI (Vector Laboratories). Confocal images were acquired using a Zeiss 530 confocal microscope (Zeiss). Results were confirmed using Western blot on whole cell lysates derived from all three cell lines, staining with anti-claudin-4 antibodies.

To investigate binding of ^{111}In-cCPE.GST to claudin-4 receptors, aliquots of 2 x 10^5 MDA-MB-468, SQ20b or HT1080 cells growing in a 24-well plate in 500 μL of growth medium were exposed to 1-1000

nM ^{111}In-cCPE.GST or ^{111}In-GST (1 MBq/μg). After incubation for 1 h at 4°C, supernatant was removed and cells were washed and lysed using 0.1 M NaOH. Cell-associated and unbound ^{111}In were measured using an automated gammacounter (Wizard^2, Perkin Elmer). To determine intracellular fate after receptor binding, cells were exposed to 500 nM ^{111}In-cCPE.GST or ^{111}In-GST. At selected times, supernatant was removed from the cells, cells were washed with 0.1 M glycine.HCl pH 2.5 to remove cell-surface bound radioactivity, and cells were lysed using 0.1 M NaOH, as previously described (*17*). Radioactivity in cytoplasmic and nuclear fractions was counted in a gammacounter. Binding affinity and the number of accessible binding sites were estimated by non-linear regression analysis with a one-site total binding model using the software package GraphPad Prism (Graphpad Software Inc). In order to study binding specificity, in some cases increasing amounts of cold, unlabelled cCPE.GST was added, to compete with the binding of 2 nM ^{111}In-cCPE.GST. IC50 values were calculated by non-linear regression with a one-site competition model with variable Hill slope using GraphPad Prism.

In Vivo Studies

All animal procedures were carried out in accordance with the UK Animals (Scientific Procedures) Act 1986 and with local ethical committee approval. MDA-MB-468 or HT1080 xenografts were established in female athymic *balb/c nu/nu* mice (Harlan). ^{111}In-cCPE.GST or ^{111}In-GST (5 MBq, 5 μg) was injected intravenously, and SPECT and CT images were acquired using a nanoSPECT-CT scanner (Bioscan) at 3 and 24 hours post injection (p.i.). Volume of interest (VOI) analysis on SPECT images was performed using the Inveon Research Workplace software package (Siemens). After imaging, mice were sacrificed and selected tissues were removed, rinsed, blot dried, weighed, and the amount of ^{111}In in each tissue was measured using an automated gammacounter. Uptake was expressed as the percentage of the injected dose per gram of tissue (%ID/g).

The ability of ^{111}In-cCPE.GST to target claudin-4 *in vivo* was further studied in the *Balb/neuT* genetically engineered mouse model of breast cancer (*18*). A more detailed description of this mouse model is presented in the supplementary methods section. ^{111}In-cCPE.GST or GST imaging was performed as described above in *balb/neuT* mice aged around 80 days, bearing aplastic lesions, or aged 120-140 days, bearing overt mammary tumors.

After imaging, sections (10 μm) were generated from snap-frozen tumour tissue harvested from xenografts and *balb/neuT* mice. Sections were stained with H&E to confirm histological status. Other sections were stained for claudin-4, using mouse anti-claudin-4 antibodies (R&D systems, clone 382321), and mounted using Vectashield containing DAPI to stain for nuclei. Images were acquired using confocal microscopy as described above.

Statistical Analyses

All statistical analyses and non-linear regression were performed using Graphpad Prism. 1 or 2-way ANOVA was used for multiple comparisons, with Tukey post-tests to calculate significance of differences between groups. All data were obtained in triplicate or more independent replicates. Results are reported and graphed as averages ± one standard deviation, unless stated otherwise.

RESULTS

Reaction of a four-fold excess of pSCN-Bn-DTPA with cCPE.GST or GST resulted in a conjugation yield of approximately 1 DTPA molecule per cCPE.GST or GST protein. ^{111}In radiolabelling yield, as determined by ITLC or G25 SEC was routinely >95% (Supplementary Figure S2).

Expression of claudin-4 on MDA-MB-468 and SQ20b, but not on HT1080 cells, was confirmed by immunocytochemistry and Western blot on whole cell lysates (Figure 1A, B). Densitometry further corroborated these results (Supplementary Figure S3A and B). Relative claudin-4 signal on immunofluorescence images was significantly higher for MDA-MB-468 and SQ20b, compared to HT1080 cells (3.74 ± 0.62, 4.24 ± 0.51, and 1.00 ± 0.11, respectively; P<0.001). Western blot signal showed a 22.2-fold and a 22.8-fold higher expression of claudin in MDA-MB-468 and SQ20b cells, respectively, compared to HT1080.

Affinity of radiolabelled cCPE-GST for claudin-4 was confirmed by binding to claudin-4 expressing MDA-MB-468 and SQ20b cells, but not to claudin-4 negative HT1080 cells (Figure 2). After exposure of cells to ^{111}In-cCPE.GST, radioactivity associated with MDA-MB-468 cells was 24.1±0.9 times higher for ^{111}In-cCPE.GST vs. ^{111}In-GST (P<0.001). Association of ^{111}In-cCPE.GST was 4.7±0.2 times higher with MDA-MB-468 vs. HT1080 cell (P<0.001). The affinity of ^{111}In-cCPE.GST for claudin-4 receptors of 1.93±0.59 μM (K_D; R^2=0.99) was comparable to earlier reported values of 0.65 μM for unmodified CPE binding to purified His_{10}-claudin-4 binding by Van Italie et al. (*14*). It was calculated that each MDA-MB-468 cell accommodates on average 3.9±0.1 million copies of ^{111}In-cCPE.GST to its extracellular surface (B_{max}). Blocking the specific binding of cCPE.GST to its receptor by addition of increasing amounts of cold, unlabelled cCPE.GST showed excellent specificity (Log[IC_{50}] = 1.3±0.07 nM; R^2=0.98) (Figure 2B).

Internalisation analysis in MDA-MB-468, SQ20b, or HT1080 cells revealed that ^{111}In-cCPE.GST, but not ^{111}In-GST, was internalised in claudin-4 positive MDA-MB-468 and SQ20b cells, but not in claudin-4

negative HT1080 cells (Supplementary Figure S4A). The amount of ^{111}In internalised into SQ20b cells was markedly higher compared to MDA-MB-468 cells (after 2 h, 0.61±0.03% of the added ^{111}In was found inside the cells, compared to 0.23±0.04% for MDA-MB-468 cells; P<0.0001), even though the amount of ^{111}In-cCPE.GST associated with the membrane of either cell was not significantly different (1.03±0.17% vs. 0.23±0.11%, respectively; P>0.05) (Supplementary Figure S4A,B).

SPECT/CT imaging of athymic *balb/c* mice carrying subcutaneous xenograft tumors revealed marked uptake of ^{111}In-cCPE.GST in MDA-MB-468 xenografts, but ^{111}In-GST uptake in MDA-MB-468 xenografts was significantly lower (6.72±0.18 vs. 3.88±1.00 %ID/g; P<0.0001). ^{111}In-cCPE.GST was taken up in HT1080 tumors at much reduced levels (2.36±1.25 %ID/g; P<0.0001) (Figure 3A). Immunohistochemistry on sections obtained from tumor tissue showed claudin-4 overexpression in MDA-MB-468, but not in HT1080 xenografts (Figure 3B), with densitometry corroborating these results (Supplementary Figure 3C). Relative claudin-4 signal was 8.2±1.5-fold higher in MDA-MB-468 xenografts, compared to HT1080 tumors (P<0.0001). SPECT imaging results were confirmed by gamma counting of tumor tissues after dissection. ^{111}In-cCPE.GST uptake in MDA-MB-468 xenografts was 6.72 ± 0.18 %ID/g, 24 hours after injection, significantly higher than ^{111}In-GST (3.88 ± 1.00 %ID/g; P<0.0001), and uptake of ^{111}In-cCPE.GST in claudin-4 negative HT1080 xenografts (2.36 ± 1.16 %ID/g; P<0.0001) (Figure 3C). Uptake in normal tissues was limited, resulting in tumor-to-muscle and tumor-to-blood ratios of 7.83±0.21 and 4.00±0.11, respectively, in MDA-MB-468 xenograft bearing mice, 24 h after injection of ^{111}In-cCPE.GST, significantly higher than ^{111}In-GST, or ^{111}In-cCPE.GST in HT1080 xenograft-bearing mice (tumor-to-muscle ratios of 4.53±1.17 and 2.98±1.57 and tumor-to-blood ratios 2.11±0.54 and 1.32±0.70, respectively; P<0.05; Figure 3C). Uptake of ^{111}In was also observed in knee and shoulder joints, potentially a result from the use of DTPA as a chelator. Some limited uptake of ^{111}In-cCPE.GST was observed in the intestines, especially the small intestine. It was also observed that uptake of ^{111}In-cCPE.GST in normal mammary fat pads in these animals is low (1.36±0.35 %ID/g).

Claudin-4 expression in established mammary tumors, harvested from 120-140 day-old *balb/neuT* mice was confirmed using immunohistochemistry (Figure 4A, Supplementary Figure S4D). Claudin-4 signal from carcinomas was 3.1±0.7-fold higher compared to normal muscle tissue. Histological stage was confirmed using H&E and anti-SMA staining (Supplementary Figure S5A and B). Established tumors, measuring 280 mm^3 on average, were clearly visualised with ^{111}In-cCPE.GST on SPECT/CT images (Figure 4B). Moreover, CT imaging could also visualise these tumors. Uptake of ^{111}In-cCPE.GST in tumor tissue in *balb/neuT* mice was significantly higher compared to ^{111}In-GST control (at 3 h post injection, uptake was 8.50±1.40 vs. 4.50±1.10 %ID/g, respectively; $P<0.01$) (Supplementary Figure 6A). Muscle uptake was limited to <2%ID/g (Supplementary Figure 6B), leading to tumor-to-muscle ratios at 24 hours post injection of 5.30±2.10 and 1.30±1.20 for ^{111}In-cCPE.GST and ^{111}In-GST, respectively ($P<0.05$) (Figure 4C). Normal tissue distribution was similar to that in athymic *balb/c* mice (Supplementary Figure 6C). No significant differences were observed between ^{111}In-cCPE.GST and GST in any of the tissues studied ($P>0.05$).

Aplastic lesions, harvested from the mammary fat pads of *balb/neuT* mice aged 80 days showed increased levels of claudin-4, compared to low-level expression in breast muscle (3.3±0.2-fold higher; $P<0.001$) and normal mammary fat pads (2.3±0.1-fold higher; $P<0.001$), harvested from wild type *balb/c* mice (Figure 5A, Supplementary Figure S3E). Histological stage was confirmed using H&E staining (Supplementary Figure S5). Representative SPECT/CT images are shown in Figure 5B. Moreover, these lesions accumulated ^{111}In-cCPE.GST (3.17±0.51 %ID/g), but not ^{111}In-GST (0.99±0.39 %ID/g; $P<0.001$) (Figure 5C). Notably, at this age, CT imaging did not reveal the presence of neoplastic tissue in any of the 6 mice studied.

DISCUSSION

Tumour-specific non-invasive molecular imaging tools have the possibility to revolutionize cancer detection, by allowing diagnosis at early stages of oncogenesis. Early diagnosis of any cancer type significantly improves the chances for survival. Although screening of the general population for all types of cancer with a single general technique is not economically feasible, the focused follow-up of high-risk patients may lead to markedly improved survival in these groups. Examples of readily identifiable risk groups include those with germ-line mutations such as BRCA1 and 2, increasing the lifetime risk of breast and ovarian cancer (*19*), or those with hereditary risks of pancreatic cancer (*20*).

Neesse et al. showed that a fluorescently labelled fragment of the naturally occurring bacterial protein, CPE, fused to GST, was able to target pancreatic cancer in several mouse models (*5*). Importantly, it was demonstrated that imaging of Pan-In precursor lesions was possible. However, although fluorescence tomography imaging allowed visualisation of claudin-4-expressing pancreatic tumours in KPC mice, this optical imaging method does not allow imaging of deep-seated lesions in human patients, given the limited penetration of infrared light. Nuclear medicine techniques can overcome this issue, and allow easy translation from preclinical to human use.

Here we demonstrate, for the first time, that a radiolabelled version of the same fusion protein, cCPE.GST, allows non-invasive imaging of claudin-4 positive tumors in two mouse models of breast cancer. As a proof-of-principle, ^{111}In-cCPE.GST uptake was evaluated in a subcutaneous tumor xenograft model, and shown to target claudin-4. Since claudin-4 is well known as the CPE receptor causing gastroenteritis in the intestinal tract, some limited uptake of ^{111}In-cCPE.GST was observed in the intestines, especially the small intestine (*5*).

Previously, Foss et al. described the use of ^{125}I-labelled anti-claudin-4 whole IgG antibodies to target claudin-4 on Colo-357 and PANC-1 xenografts in mice (*21*). This resulted in tumor-to-muscle uptake ratios of 4.3 and 6.3, respectively. However, these values were obtained after 4 and 6 days after

administration of the labelled antibody, which is undesirable for clinical translation. Cy5.5-cCPE.GST signal in claudin-4 positive CAPAN-1 xenografts was approximately 2-fold higher than in claudin-4 negative HT1080 xenografts. Our results using the MDA-MB-468 xenograft model yielded average tumor-to-muscle ratios of 8:1, and a 3-fold higher uptake compared to HT1080 tumors, reached at 24 hours post injection. These results are very positive, especially in light of a relatively unfavourable K_d. We hypothesize that the main factor influencing the high tumor uptake of ^{111}In-cCPE.GST may be the high number of cCPE receptors, calculated as 3.9±0.1 million per cell. To aid clinical translation, optimisation of the binding affinity to claudin-4 may be necessary, for example through biochemical modification.

Given the well-known disadvantages associated with xenograft models (these disadvantages are reviewed in great detail elsewhere (*22*)), we set out to validate ^{111}In-cCPE.GST SPECT imaging in a genetically engineered mouse model of breast cancer, since these more faithfully represent human disease (*18*). Since cancer progression in *balb/neuT* mice mimics that of HER2-positive ductal carcinoma in situ (DCIS), the use of this spontaneous cancer model allowed us to study claudin-4 imaging during tumorigenesis. Our imaging results in *balb/neuT* animals revealed tumor-to-muscle ratios of 4.8:1, even at 3 hours post injection. Even though absolute tumor uptake levels decreased from 8.50±1.40%ID/g to 3.20±0.70%ID/g at 24 h post injection, tumor-to-muscle increased to 5.3:1. Tumor uptake levels in *balb/neuT* mice were lower compared to the xenograft studies, but nevertheless reflect the expression of the target epitope, claudin-4, on the tumor versus normal tissues such as normal fat pad tissue or breast muscle tissue (Figure 5).

Overt tumors in *balb/neuT* mice were clearly visible on CT images. On the contrary, aplastic lesions, by their very nature were too small to be detected using anatomical CT imaging. Since claudin-4 expression is upregulated at this early stage of tumor progression, ^{111}In-cCPE SPECT imaging allowed good visualisation of preneoplastic lesions, at least in this tumor model. Given that tumors in this mouse model are only palpable on average when mice reach approximate ages of 130 days (*18*), SPECT imaging allows

detection almost 40% (50 days) earlier, in mice aged 80 days, and prior to CT imaging. Given that X-ray imaging is currently used as the preferred method of breast cancer screening, our method of very early detection may enable even earlier therapeutic intervention, or trigger more frequent follow-up of patients at risk. Here, we have described a SPECT imaging method for claudin-4 imaging, but since PET imaging has a much increased sensitivity compared to SPECT, and PET results can be more easily quantified, a translation of the SPECT imaging method described here to PET imaging using alternative radioisotopes such as ^{89}Zr or ^{64}Cu would facilitate clinical translation. A limitation for clinical translation may be the potential immunoreactivity of cCPE. Currently, little information is available on the humoral response of humans to *C. perfringens* A toxins and the prevalence of preformed antibodies in the general population (*23*) Although we and others did not observe any adverse reactions in mice following repeated cCPE dosing (*24*), the safety and antigenicity of cCPE must be evaluated for future clinical application, especially in individuals with a history of *C. perfringens*-induced enteritis or after repeated exposure to cCPE as immune reactions due to preformed antibodies cannot be ruled out completely.

Claudins in general and claudin-4 in particular have a known involvement in epithelial-to-mesenchymal transition (EMT), the complex stepwise phenomenon that occurs during both embryonic development and very early during tumorigenesis (*25*). A recent link between EMT and cancer stem cells (CSCs) has sparked considerable interest, since it is widely accepted that only a minor population of tumor cells can initiate and support the development of tumors, and the highly aggressive tumor cells share many characteristics of embryonic progenitor cells. Given that the crucial proteins snail, slug and E-cadherin are involved in claudin regulation, it is tempting to link claudin-4-targeted imaging to early detection of EMT. However, the limited amount of available evidence warrants further investigation in order to formally validate this association. Compared to other well-studied biomarkers, such as HER2, PR and ER in breast cancer, claudin-4 (and -3) are less well understood, and the mechanisms that drive the intricate correlation between claudins and tumor progression remain a topic of intense research. Therefore, a better understanding of the role of claudins in tumorigenesis, tumor progression, EMT and CSCs may provide

important information to elucidate the molecular mechanisms that underpin the use of claudins as imaging biomarkers and aid in the design of new imaging agents or multimodal imaging biomarkers (*3*).

Taken together, ^{111}In-labelled cCPE.GST is an improved agent for the imaging of claudin-4 positive tumorous lesions. Possible applications might include its use as an imaging biomarker for early detection cancer and (pre-)neoplasms, with applications in screening of breast, ovarian, lung, and pancreatic cancer (*3*). Previously reported data also demonstrate that claudin-4 positivity is retained in metastases, at least in the KPC murine pancreatic cancer model (*5*), and claudin-4 SPECT or PET imaging may be useful as a follow-up procedure to detect recurrent disease after curative therapies.

CONCLUSION

^{111}In-cCPE.GST targets claudin-4 expression in frank tumors and preneoplastic tissue in *balb/neuT* mice. cCPE imaging may be used as an early detection tool for cancer of the breast, prostate, or pancreas.

ACKNOWLEDGMENTS

The authors would like to thank Cancer Research UK, MRC and the EPRSC/CRUK Cancer Imaging Centre in Oxford, for financial support, and Prof. Yasuhiko Horiguti at Osaka University for his support. AN is supported by a Max Eder fellowship from the Deutsche Krebshilfe.

REFERENCES

1. Fass L. Imaging and cancer: a review. *Mol Oncol.* 2008;2:115-152.

2. Neesse A, Griesmann H, Gress TM, Michl P. Claudin-4 as therapeutic target in cancer. *Arch Biochem Biophys.* 2012;524:64-70.

3. Kwon MJ. Emerging roles of claudins in human cancer. *Int J Mol Sci.* 2013;14:18148-18180.

4. Kulka J, Szasz AM, Nemeth Z, et al. Expression of tight junction protein claudin-4 in basal-like breast carcinomas. *Pathol Oncol Res.* 2009;15:59-64.

5. Neesse A, Hahnenkamp A, Griesmann H, et al. Claudin-4-targeted optical imaging detects pancreatic cancer and its precursor lesions. *Gut.* 2013;62:1034-1043.

6. Landers KA, Samaratunga H, Teng L, et al. Identification of claudin-4 as a marker highly overexpressed in both primary and metastatic prostate cancer. *Br J Cancer.* 2008;99:491-501.

7. Shang X, Lin X, Alvarez E, Manorek G, Howell SB. Tight junction proteins claudin-3 and claudin-4 control tumor growth and metastases. *Neoplasia.* 2012;14:974-985.

8. Ersoz S, Mungan S, Cobanoglu U, Turgutalp H, Ozoran Y. Prognostic importance of Claudin-1 and Claudin-4 expression in colon carcinomas. *Pathol Res Pract.* 2011;207:285-289.

9. Kominsky SL, Vali M, Korz D, et al. Clostridium perfringens enterotoxin elicits rapid and specific cytolysis of breast carcinoma cells mediated through tight junction proteins claudin 3 and 4. *Am J Pathol.* 2004;164:1627-1633.

10. Lanigan F, McKiernan E, Brennan DJ, et al. Increased claudin-4 expression is associated with poor prognosis and high tumour grade in breast cancer. *Int J Cancer.* 2009;124:2088-2097.

11. Michl P, Buchholz M, Rolke M, et al. Claudin-4: a new target for pancreatic cancer treatment using Clostridium perfringens enterotoxin. *Gastroenterology.* 2001;121:678-684.

12. Robertson SL, McClane BA. Interactions between Clostridium perfringens enterotoxin and claudins. *Methods Mol Biol.* 2011;762:63-75.

13. Hanna PC, Wnek AP, McClane BA. Molecular cloning of the 3' half of the Clostridium perfringens enterotoxin gene and demonstration that this region encodes receptor-binding activity. *J Bacteriol.* 1989;171:6815-6820.

14. Van Itallie CM, Betts L, Smedley JG, 3rd, McClane BA, Anderson JM. Structure of the claudin-binding domain of Clostridium perfringens enterotoxin. *J Biol Chem.* 2008;283:268-274.

15. Cocco E, Casagrande F, Bellone S, et al. Clostridium perfringens enterotoxin carboxy-terminal fragment is a novel tumor-homing peptide for human ovarian cancer. *BMC Cancer.* 2010;10:349.

16. Hnatowich DJ, Layne WW, Childs RL. The preparation and labeling of DTPA-coupled albumin. *Int J Appl Radiat Isot.* 1982;33:327-332.

17. Cornelissen B, Hu M, McLarty K, Costantini D, Reilly RM. Cellular penetration and nuclear importation properties of 111In-labeled and 123I-labeled HIV-1 tat peptide immunoconjugates in BT-474 human breast cancer cells. *Nucl Med Biol.* 2007;34:37-46.

18. Quaglino E, Mastini C, Forni G, Cavallo F. ErbB2 transgenic mice: a tool for investigation of the immune prevention and treatment of mammary carcinomas. *Curr Protoc Immunol.* 2008;Chapter 20:Unit 20 29 21-20 29-10.

19. Antoniou A, Pharoah PD, Narod S, et al. Average risks of breast and ovarian cancer associated with BRCA1 or BRCA2 mutations detected in case Series unselected for family history: a combined analysis of 22 studies. *Am J Hum Genet.* 2003;72:1117-1130.

20. Klein AP, Hruban RH, Brune KA, Petersen GM, Goggins M. Familial pancreatic cancer. *Cancer J.* 2001;7:266-273.

21. Foss CA, Fox JJ, Feldmann G, et al. Radiolabeled anti-claudin 4 and anti-prostate stem cell antigen: initial imaging in experimental models of pancreatic cancer. *Mol Imaging.* 2007;6:131-139.

22. Richmond A, Su Y. Mouse xenograft models vs GEM models for human cancer therapeutics. *Dis Model Mech.* 2008;1:78-82.

23. Zaren E, Schwan A, Frenckner B. Age related variations of serum concentrations of normally occurring IgG antibodies to Clostridium perfringens. *J Clin Pathol.* 1987;40:282-285.

24. Suzuki H, Kondoh M, Li X, et al. A toxicological evaluation of a claudin modulator, the C-terminal fragment of Clostridium perfringens enterotoxin, in mice. *Pharmazie.* 2011;66:543-546.

25. Wang Y, Zhou BP. Epithelial-mesenchymal transition in breast cancer progression and metastasis. *Chin J Cancer.* 2011;30:603-611.

Figure 1

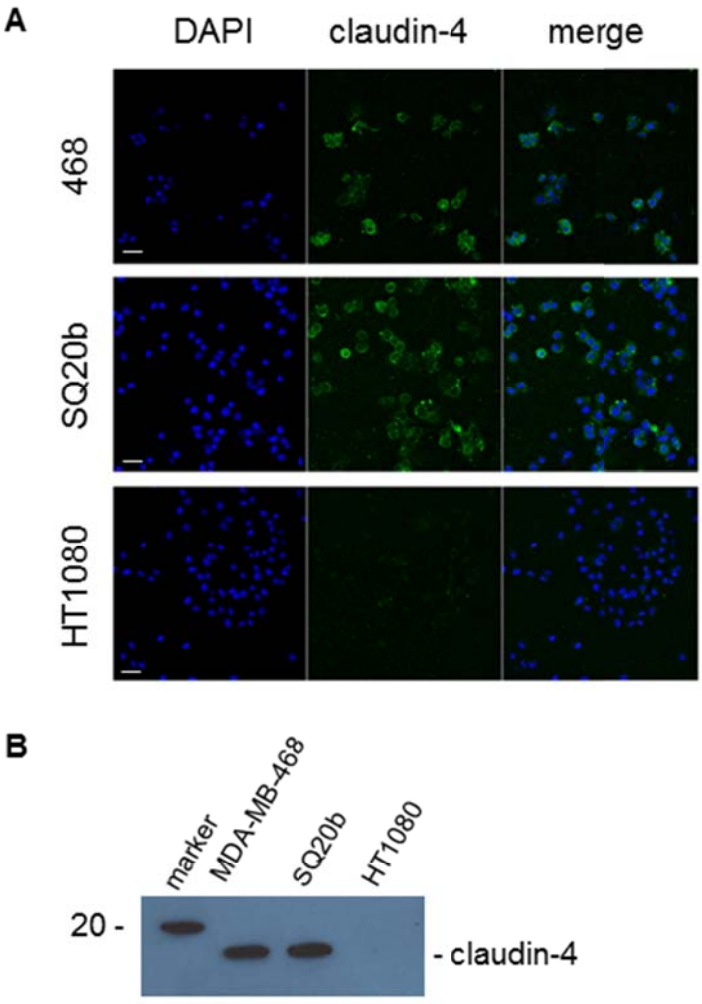

Figure 1. (A) MDA-MB-468, SQ20b, and HT1080 cells were stained for claudin-4. Scale bar: 20 µm. (**B**) Western blot demonstrating presence or absence of claudin-4 in whole cell lysates obtained from MDA-MB-468, SQ20b, and HT1080 cells.

Figure 2

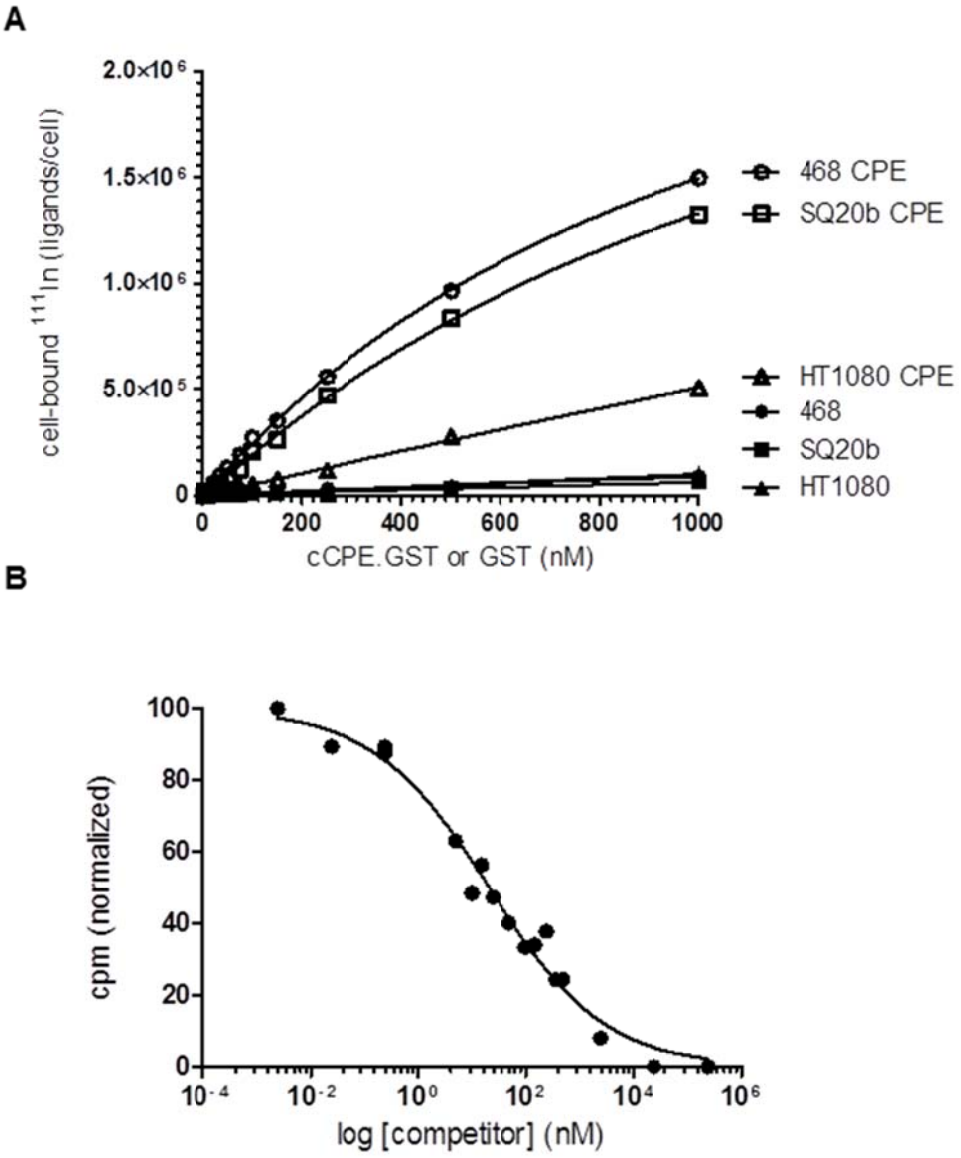

Figure 2. (A) MDA-MB-468 cells were exposed for 1 hour at 4°C to increasing concentrations of ^{111}In-labelled cCPE.GST or GST, and the extent of cell-binding was determined. (**B**) Increasing amounts of unlabelled cCPE.GST were used to block the binding of ^{111}In-cCPE.GST to MDA-MB-468 cells.

Figure 3

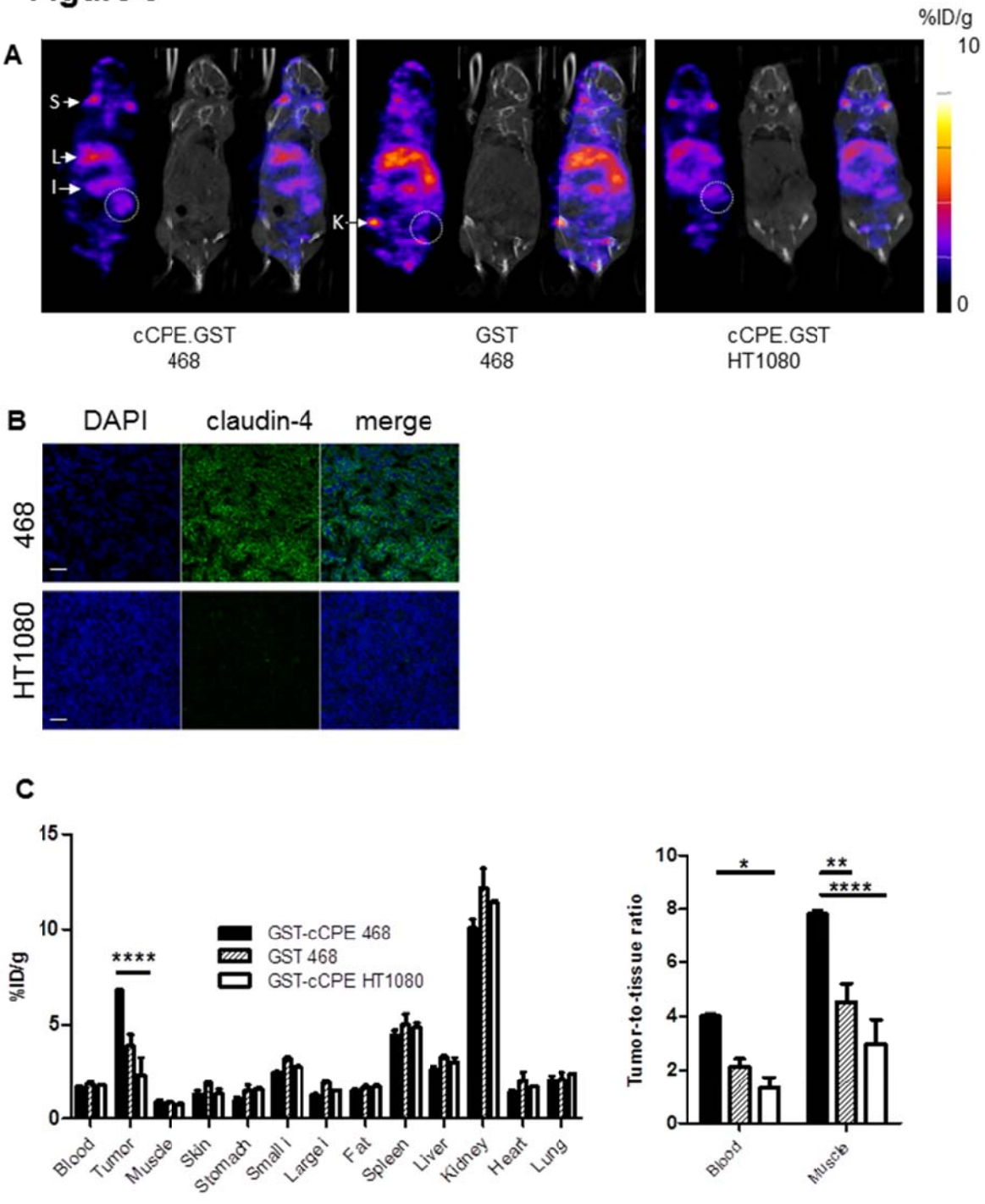

Figure 3. (**A**) Representative SPECT/CT images of mice carrying tumor xenografts (white circles) of MDA-MB-468 (claudin-4 positive) or HT1080 (claudin-4 negative) cells, 24 hours after intravenous administration of ^{111}In-cCPE.GST or ^{111}In-GST. ^{111}In-uptake was also observed in shoulder joints (S),

liver (L), intestines (I), and knee joints (K). Coronal sections through the tumor are shown. (**B**) Sections obtained from MDA-MB-468 or HT1080 xenograft tumors were stained using anti-claudin-4 antibodies. Scale bar: 20 μm. (**C**) Biodistribution results, 24 h post intravenous administration of ^{111}In-cCPE.GST or ^{111}In-GST. Tumor-to-blood and tumor-to-muscle ratios were calculated. Each group contained at least three animals.

Figure 4

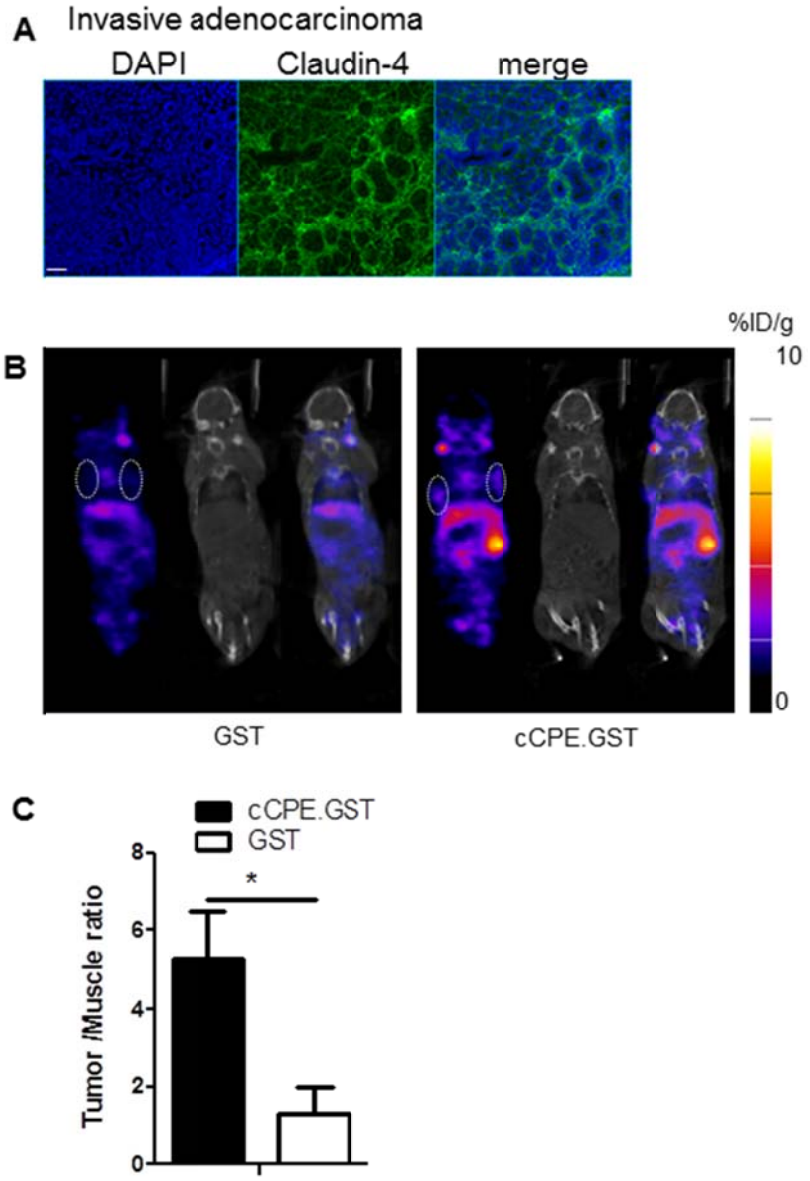

Figure 4. (**A**) Sections obtained from tumors harvested from a 139 day old *balb/neuT* mouse were stained using anti-claudin-4 antibodies. Scale bar: 20 µm. **(B)** Representative SPECT/CT images of *balb/neuT* mice, aged 139 days, bearing mammary tumors (white circles), 24 hours after intravenous administration of ^{111}In-cCPE.GST or ^{111}In-GST. Overt tumors were clearly visible on CT images. Coronal sections

through the tumor are shown. (**C**) VOI analysis of *balb/neuT* mice bearing overt tumors 3 or 24 hours post injection of ^{111}In-cCPE.GST or ^{111}In-GST. Each group contained at least three animals.

Figure 5

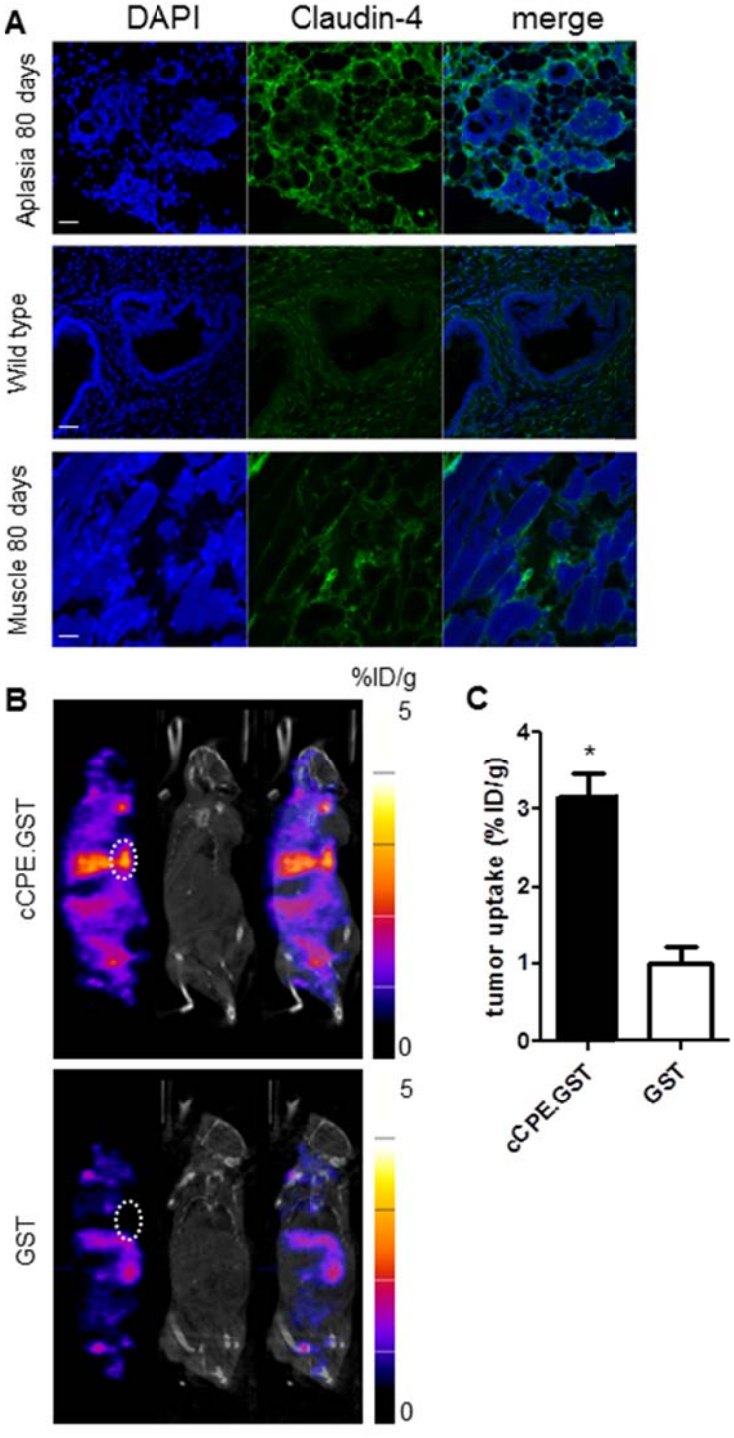

Figure 5. (**A**) Sections obtained from aplastic lesion or muscle harvested from a 80 day old *balb/neuT* mouse, or ductal tissue obtained from a wild-type *balb/c* mouse were stained using anti-claudin-4

antibodies. Scale bar: 20 μm. (**B**) Representative SPECT/CT images of *balb/neuT* mice, aged 80 days, bearing aplastic lesions (white circles), 24 hours after intravenous administration of ^{111}In-cCPE.GST or ^{111}In-GST. Functional SPECT imaging was compared to anatomical CT imaging. Aplastic lesion could not be detected on CT images. Coronal sections through mammary fat pads are shown. (**C**) VOI analysis of 80 day old *balb/neuT* mice bearing aplastic 24 hours post injection of ^{111}In-cCPE.GST or ^{111}In-GST. Each group contained at least three animals.